Title
3D printed microfluidic devices for circulating tumor cells (CTCs) isolation

Authors
Chen, Juhong
Liu, Chun-Yen
Wang, Xinchang
et al.

Publication Date
2020-02-01

DOI
10.1016/j.bios.2019.111900

Peer reviewed

HHS Public Access

Author manuscript

Biosens Bioelectron. Author manuscript; available in PMC 2022 July 08.

Published in final edited form as:

Biosens Bioelectron. 2020 February 15; 150: 111900. doi:10.1016/j.bios.2019.111900.

3D printed microfluidic devices for circulating tumor cells (CTCs) isolation

Juhong Chen[a,b,c,d,1,*], **Chun-Yen Liu**[e,f,1], **Xinchang Wang**[a,g], **Eric Sweet**[a,b], **Nathaniel Liu**[a], **Xiaohua Gong**[e], **Liwei Lin**[a,b,**]

[a]Department of Mechanical Engineering, University of California, Berkeley, USA

[b]Berkeley Sensor and Actuators Center, USA

[c]Department of Biological Systems Engineering, Virginia Tech, USA

[d]Hangzhou Institute of Advanced Transducing Technology, Wahaha R&D Academe, Hangzhou, China

[e]School of Optometry and Vision Science Program, University of California, Berkeley, USA

[f]Department of Materials Science and Engineering, National Cheng Kung University, Tainan, Taiwan

[g]School of Mechanical Engineering, Shanghai Jiao Tong University, Shanghai, China

Abstract

Isolation of circulating tumor cells (CTCs) from blood samples has important prognostic and therapeutic implications for cancer treatments, but the process is very challenging due to the low concentration of CTCs. In this study, we report a novel 3D printed microfluidic device functionalized with anti-EpCAM (epithelial cell adhesion molecule) antibodies to isolate CTCs from human blood samples. A 3D printing technology was utilized with specially designed interior structures to fabricate a microfluidic device with high surface area and fluid flow manipulation, increasing capture efficiency of tumor cells. These devices with the optimal flow rate (1 mL/h) and channel length (2 cm) were demonstrated to test three kinds of EpCAM positive cancer cell lines (MCF-7 breast cancer, SW480 colon cancer, and PC3 prostate cancer), and one kind of EpCAM

[*]Corresponding author. Department of Biological Systems Engineering, Virginia Tech, Blacksburg, USA. jhchen@vt.edu (J. Chen).
[**]Corresponding author. Department of Mechanical Engineering, University of California, Berkeley, USA. lwlin@berkeley.edu (L. Lin).
[1]These authors contributed equally to this work.

Declaration of competing interest

The authors declare that they have no known competing financial interests or personal relationships that could have appeared to influence the work reported in this paper.

CRediT authorship contribution statement

Juhong Chen: Conceptualization, Methodology, Validation, Formal analysis, Investigation, Data curation, Writing - original draft, Writing - review & editing, Project administration. **Chun-Yen Liu:** Conceptualization, Methodology, Validation, Data curation, Writing - review & editing, Visualization. **Xinchang Wang:** Software, Formal analysis, Data curation, Writing - review & editing, Visualization. **Eric Sweet:** Resources, Writing - review & editing, Visualization. **Nathaniel Liu:** Methodology, Resources, Writing - review & editing. **Xiaohua Gong:** Data curation, Writing - review & editing, Supervision. **Liwei Lin:** Conceptualization, Validation, Data curation, Writing - review & editing, Supervision, Project administration, Funding acquisition.

Appendix A. Supplementary data

Supplementary data to this article can be found online at https://doi.org/10.1016/j.bios.2019.111900.

negative cancer cell line (293T kidney cancer). Experimentally, the capture efficiency higher than 90% has been achieved, and the isolation of MCF-7 tumor cells from spiked human blood samples has also been demonstrated. Combined with DNA-based detection (e.g. polymerase chain reaction or DNA sequencing), the detection and analysis of released DNAs from captured tumor cells could be another future direction for clinical diagnosis and cancer treatment.

Keywords

3D printing; Circulating tumor cell (CTC); Microfluidic separation; Immunocapture; Diagnostics

1. Introduction

Cancer metastasis causes 90% of all cancer-related deaths(Park et al., 2016). In these cases, cancer cells are able to detach from a tumor and enter blood vessels to circulate in human fluids(Chen et al., 2014; Cheng et al., 2015; Jackson et al., 2017). These tumor cells are called circulating tumor cells (CTCs), which have the potential to invade and colonize at distal sites, resulting in fatal metastasis(Nagrath et al., 2007; Wu et al., 2017). In the recent years, CTCs from the peripheral blood of patients have been reported in the liquid-based biopsy as biomarkers for the detection of various cancers, such as breast, prostate, and liver cancer(Miller et al., 2010; Pantel and Alix-Panabières, 2013; Riethdorf et al., 2010). Furthermore, the enumeration of CTC counts during a specific cancer treatment process has been used to monitor the effectiveness of treatment-resistance progression(Kurkuri et al., 2011; Wu et al., 2014). Thus, there is an urgent need to advance the study of CTC isolation and detection to enable both early diagnostics and treatment progresses.

The major challenge for the isolation and detection of CTCs in bloodstream is their extremely low concentration (less than 100 cells per mL) as compared to native blood cell concentration ($>10^9$ cells per mL) (Gleghorn et al., 2010; Talasaz et al., 2009). The enrichment of CTCs is beneficial for cancer diagnostics and treatment such that a diverse array of technologies have been developed to address this task. Most of these techniques can be classified as (1) label-free and (2) affinity-based isolation of CTCs(Li et al., 2015; Murlidhar et al., 2016). Several methodologies have been demonstrated to separate CTCs in the label-free route, such as filtration, hydrodynamic chromatography, and dielectrophoresis (Earhart et al., 2014; Li et al., 2015; Sun et al., 2012; Wang et al., 2011). For example, Shah et al. have reported the capture of cells in microfluidic chip based on the positive-dielectrophoresis approach(Shah et al., 2014). But they often fail to achieve a high purity of CTCs and compromise cell viability for postprocessing analysis. Currently, affinity-based microfluidic devices have attracted significant attention for CTC studies(Lin et al., 2014; Reategui et al., 2015; Yoon et al., 2016). A variety of 3D microstructures have been proposed to increase the surface area and fluid flow manipulation to result in high CTC capture efficiency(Ahmed et al., 2017; Murlidhar et al., 2014; Nagrath et al., 2007; Sarioglu et al., 2015). For example, Nagrath et al. have reported antibody-functionalized micropillars within microfluidic channels to isolate CTCs(Nagrath et al., 2007). Assorted micropillar geometries have been investigated by Ahmed et al. to increase the CTC capture efficiency(Ahmed et al., 2017). While these microfluidic systems can capture and separate

CTCs from peripheral blood, their lithography-based fabrication processes are complex and time-consuming.

The most conventional approaches to fabricate microfluidic devices are based on molding techniques involving poly(dimethylsiloxane) (PDMS) and other thermoplastics(Au et al., 2014; Sackmann et al., 2014). The disadvantages using the conventional approaches have limited their wide applications, such as the requirement of cleanroom-based fabrication, high cost and time-consuming of wafer processes, and labor intense of manual assembling multiple layers(Au et al., 2014; Chen et al., 2015b; Sochol et al., 2016; Tseng et al., 2014). In addition, it is difficult to efficiently fabricate true 3D structures with high surface areas to increase the capture efficiency of CTCs. In the past few years, 3D printing, which can create 3D objects layer-by-layer, has received wide attention as a potential alternative to the PDMS-based conventional molding process.(Au et al., 2016; Bhattacharjee et al., 2016; Chan et al., 2017; Sochol et al., 2016). To the best of our knowledge, 3D printed microfluidics have not been fabricated to isolate CTCs.

In this study, a microfluidic device was fabricated using 3D printing technology to isolate CTCs from peripheral blood samples. The inner surfaces were successfully functionalized with antibodies to provide capture sites for tumor cells with a designed fluid flow to maximize CTC-antibody interactions in the microfluidic channels. The influences of structural design, fluid flow rate, and channel length were investigated and optimized to increase the capture efficiency of CTCs. The devices under the optimized conditions were demonstrated to capture CTCs from artificially-spiked blood samples, which can later be integrated into a larger scale 3D printed network for cancer diagnostic and treatment applications.

2. Experimental section

Chemicals, materials, and instrumentation.

3D printed materials (20–40% of proprietary, 15–35% of ethoxylated bisphenol A diacrylate, and 1.5–3% of tripropyleneglycol diacrylate) and wax-based ink were purchased from 3D Systems. Dopamine hydrochloride, streptavidin, and bovine serum albumin (BSA) were purchased from Sigma Aldrich. Biotinylated anti-EpCAM antibodies were purchased from Abcam. MCF-7 tumor cells were obtained from cell culture facility at the University of California, Berkeley. All other analytical grade chemicals were purchased from Fisher Scientific. The Milli-Q water with 18 MΩ/cm was used for the preparation all solution. The microfluidic devices were printed using a ProJet 3000HD 3D printers (3D systems). The SEM images were captured using FEI Quanta 3D PEG FIB. The fluorescent and brightfield images were captured using Zeiss LSM 700 confocal laser scanning microscopy (CLSM).

3D printed microfluidic device fabrication.

3D printed microfluidic devices were designed using 3D modelling CAD (SolidWorks) and fabricated using a ProJet 3000HD 3D printers (3D systems) according to previously reported steps with minor modifications(Sochol et al., 2016). On the Ultra High Definition print configuration, this printer enabled an approximately 40 μm resolution in the horizontal

plane of the 3D printing process, and slightly better (approximately 30 μm) resolution in the vertical direction. Briefly, 3D models of the microfluidic devices in the STL file format (a standard file type for high-quality 3D models) were imported into the ProJet Accelerator software (3D systems). Under precise digital control, the devices were printed with the one open face in contact with the printbed, and printed in parallel such that the printer's primary raster function (laterally across the printbed) traversed the width of the devices rather than their length to enable a more uniform print in the cross-section of the flow inputs. Specifically, microfluidic devices were printed by depositing either photocurable plastic resin or casting wax support materials layer-by-layer using two different printer nozzles (one for the photoplastic build material and the other one for sacrificial wax support material). Following the 3D printing process, the devices were immersed into food grade mineral oil at 65 °C and the internal wax were removed using a syringe. Lastly, pressurized air was used to evacuate the remaining mineral oil and dry the devices.

Inner structure modification.

Schematic illustration of the surface chemical modification and anti-EpCAM antibody immobilization procedures are depicted in Fig. 1. Briefly, dopamine solution (1 mg/mL in 10 mM Tris buffer, pH 8.5) was pumped through the channel for 1 h under a constant flow rate (1 mL/h). In alkaline solution (pH 8.5), dopamine was self-polymerized into poly(dopamine) to coat the inner structures. After washing three times using phosphate buffered saline (PBS), streptavidin solution (20 μg/mL in PBS) was pumped for another 1 h under the same flow rate. Afterward, active sites were blocked with bovine serum albumin (BSA, 3% in PBS) to avoid non-specific binding. Finally, biotinylated anti-EpCAM antibodies (10 μg/mL in PBS) were introduced to functionalize the inner surface areas via biotin-streptavidin interactions. The prepared devices were stored in PBS with 3% BSA in a refrigerator until use.

Cell capture simulations.

FLUENT module in the ANSYS WORKBENCH software was employed to perform simulations of cell capture based on the finite volume method (FVM), k-ε turbulence model, and discrete phase model (DPM). The channels were oriented vertically with the inlet downward and the gravitational acceleration was defined as 9.8 m/S^2. The continuous phase was defined using water with the inlet velocity of 0.0003 m/S according to the flow rate of 1 mL/h. The discrete phase (cell) was defined as solid particles with an average diameter of 20 μm and a total flow rate of 9.32×10^{-9} kg/S according to the cell concentration of 1×10^6 cells/mL. The density of the discrete phase was approximately defined as 1060 kg/m^3. All the solid particles were injected into the channel from the inlet and distributed evenly on the surface.

Cell culture and preparation.

Human breast cancer cell line MCF-7 (passage 2–5) was cultured using DMEM + GlutaMAX (Dulbecco's Modified Eagle's Medium) with supplements (10% fetal bovine serum, 1% penicillin-streptomycin, 1% non-essential amino acid, and 1% sodium pyruvate). Cell culture was placed in an incubator at 37 °C with 5% CO_2, and the medium was renewed every two days. Cancer cells were then suspended and harvested using 0.05%

trypsin. Immediately before the cell capture test, cells were washed and resuspended in PBS buffer. The concentration of cells was characterized using a hemocytometer. Other tumor cell lines (SW480, PC3, and 293T) were cultured in their relative media based on the ATCC® recommendations, and cells were harvested using procedures analogous to the aforementioned method for MCF-7 cells.

CTC capture and analysis.

The cell capture experiments were performed using antibody-modified 3D printed microfluidic devices. Cell lines (MCF-7, SW480, PC3, or 293T) in PBS were adjusted to the concentration of 1×10^6 cells/mL. Cell suspensions in syringes were pumped through using the Cole-Parmer tubing at room temperature. Outlet solutions containing unbound cells were collected, and the cell concentrations were also estimated using hemocytometry. Unlike the planar architecture, 3D printed devices make microscopy difficult to directly count the captured cells(Lin et al., 2017; Nagrath et al., 2007). Thus, cell capture efficiency was computed based on (total CTCs – escaped CTCs)/total CTCs. All experiments were repeated at least three times.

Blood sample analysis.

A whole blood sample from a healthy donor was collected and stored in EDTA coated tubes for use within 48 h. Human breast cancer cell line MCF-7/GFP was cultured and prepared using the above-mentioned methods. The harvested cells (1×10^6 cells/mL) were spiked into the whole blood sample without any further treatment. The artificial patient blood sample was then pumped through the anti-EpCAM antibody modified 3D printed microfluidic device. Fluorescence and brightfield images were captured using confocal laser scanning microscopy (CLSM) to determine the number of tumor cells with GFP expression and blood cells, respectively.

Statistical analysis.

All data are presented as mean ± standard deviation (SD) from at least three experimental datasets. The student t-test using SigmaPlot 12 software was conducted to determine if each set of data was significantly different from the corresponding control set. One asterisk (*) indicates a difference ($0.01 < p < 0.05$) and two asterisks (**) represents a significant difference ($p < 0.01$) between the two compared sets of data.

3. Results and discussion

3.1. Surface modification of 3D printed microfluidic device for CTC capture

In order to produce antibody-specific interaction and capture CTCs, the inner surfaces are modified using a layer-by-layer coating method (Fig. 1). Mussel-inspired self-polymerization of dopamine in alkaline solution (pH 8.5) was applied to generate a biocompatible nanostructured polydopamine (PDA) coating on the inner surface(Lee et al., 2007; Lynge et al., 2011). There are two reasons for the polydopamine coating: (1) this reaction provides a simple surface coating to virtually any materials and (2) its amine and catechol groups ease bioconjugation of other molecules. In this study, reactive sites on the PDA coating provide accessible covalent anchors for streptavidin to enable the

immobilization of biotinylated anti-EpCAM antibodies as interfaces to capture specific CTCs(Lee et al., 2009; Zhang et al., 2016). Excess active sites were blocked with BSA proteins to prevent non-specific binding. The surface morphology of 3D printed materials after different modifications were characterized using scanning electron microscopy (SEM) images. As shown in Fig. S1a, the changes of surface morphology are observed after each modification step. Based on our previous study, the polydopamine could generate a coating with thickness of 50–100 nm, which made the differences between bare- and polydopamine-coating (Chen et al., 2015a). However, the streptavidin and antibodies are small proteins (less than 10 nm), which resulted in the similar morphology among polydopamine-, streptavidin-, and antibody-coatings. As reported in the previous publications, the wettability of the inner surface would affect the cell capture efficacy because the hydrophilicity of the 3D printed materials increased water retention, preventing cell-inner structure interactions and decreasing nonspecific cell adhesion(Li et al., 2015). The surface roughness of ±95 μm in-plane and ±31 μm out-of-plane was reported in our previous publication(Sochol et al., 2016). As shown in Fig. S1b, the contact angles after each surface modification were measured to slightly change from 99.12° ± 0.55, 104.16° ± 1.46, 97.15° ± 1.29, to 91.47° ± 2.79 for bare, polydopamine-coated, streptavidin-coated, and antibody-coated surfaces, respectively.

3.2. Characterisation of CTC capture after each surface modification of 3D printed surface

The effectiveness to capture CTCs was studied experimentally. In this study, 3D printed materials after each surface modification were incubated with MCF-7 cells (1×10^6 cells/mL) in PBS at room temperature for 30 min. After washing three times to remove cells that did not attach strongly to the surfaces, tumor cells on 3D printed materials were characterized using SEM images. As shown in Fig. 2a, tumor cells are highlighted with blue color. Due to the physical attachment, tumor cells appeared to be plump spheroids affixed to the surfaces (Figs. 2a–1 and 2a-3). On the contrary, as shown in Fig. 2a-2 and 2a-4, tumor cells appear flattened with flagellum attached onto the material surface (indicated by red arrows) due to specific recognition.

The numbers of tumor cells attaching on 3D printed surfaces after each modification step were enumerated using confocal fluorescent images. Nuclear acids of tumor cells were stained using 4′,6-diamidino-2-phenylindole (DAPI) to be blue color and imaged using CLSM (Fig. 2b). Five images at 20× magnification were randomly picked and the tumor cell counts on each image were averaged (Fig. 2c). In comparison to bare (unmodified) surface, the surface with polydopamine modification can increase the cell capture rate. As reported in the previous publications, catecholamine groups could capture all kinds of cells (including blood cells) by the amine groups, resulting in non-specific capture(Ku et al., 2010). After the active surface were coated with streptavidin blocked with the bovine serum albumin (BSA), fewer tumor cells were captured. The modification of anti-EpCAM antibodies provided specific bindings to tumor cells with the EpCAM antigens and the number of captured tumor cells significantly increased.

3.3. Inner design of 3D printed microfluidic device

Prior to isolate CTCs, the 3D microfluidic devices were optimized to maximize the interactions between tumor cells and functionalized inner surfaces by (1) increasing the surface areas and (2) manipulating fluid flow. Fig. 3a shows the design of a reference structure with a 2.75 × 2.75 × 10 mm^3 chamber without inner geometries as model #0, which has a surface area of 190 mm^2. A total of 12-layer vertical bars (in model #1 and #2) and 12-layer mesh-like structure (in model #3 and #4) were added into the fluidic chamber to increase the total surface areas to 350 mm^2 and 404 mm^2, respectively. The dimensions of each layer are labeled in Fig. 3a. In order to increase cell capture efficacy, the flow pattern and speed in these designs were simulated (Fig. 3b). For models #1 and #3, the inner patterns are aligned with each other in different rows such that cells are less likely to get in contact with the surface on the backside of the bars, and less effective cell capture efficacy is expected, which is consistent with the previous reports(Nagrath et al., 2007). For models #2 and #4, the odd patterns are shifted by 500 μm (lateral shift in model #2 and both lateral and vertical shifts in model #4) to introduce interpose features within the directions of the fluidic flows. Compared with model #1 and #3, model #2 and #4 can decrease local velocity (especially model #4), improving the interactions between cells and surfaces of inner structures, respectively. These results indicated that the model #4 has the huge potential to increase the interaction between tumor cells and microfluidic inner structures.

3.4. Simulation and experimental results for CTC capture

The simulation and experimental results for CTC capture are compared in Fig. 4. All simulation parameters related to cell capture efficiency were defined based on actual experimental conditions. The simulated trajectories of particles traveling in the microfluidic systems of different models are shown in Fig. 4a. The particle intensity at the outlet layer was shown in Fig. 4b. There are fewer particles observed in the outlet of model #4, indicating higher cell capture efficiency. In simulation, the particles were captured when they contacted the inner structure for the first time, which was used to calculate capture efficiency. In reality, the particles could be captured for the second or third contact with the inner structures. As shown in Fig. 4c, experimental capture efficiencies were lower than simulation results because the particles could not be captured for the first-time contact. Similar capture efficiencies were observed for model #2 and #4, which both had the shift patterns, indicating that the capture efficiency can be increased by increasing surface area and manipulating fluid flow. Although there are some differences in capture efficiency between simulation and experiment results, experimental results show a similar trend as the simulation results with lower capture efficiency values in all models (Fig. 4c). Based on these results, model #4 will be used for the future CTC isolation in human blood samples.

3.5. Optimization of CTC capture

In order to further improve the cell capture efficiency, experimental settings (flow rate and channel length) were investigated using model #4 (Fig. 5a–b). For flow rate, the capture efficiencies as high as 88.79 ± 3.52% and 84.19 ± 3.44% were obtained at flow rates of 0.5 and 1 mL/h, respectively. It was observed that higher flow speed could result in the

decreasing of the capture efficiency, and when the flow rate reached 3 mL/h, the efficiency dramatically dropped to 19.52 ± 8.96%. Since there was no significant difference (p-value = 0.12) in terms of capture efficiency between flow rates of 0.5 and 1 mL/h, the flow rate of 1 mL/h was chosen in this work for subsequent experiments. Similarly, the capture efficiencies are significant differences (p-value = 0.005) between the channel length of 1 and 2 cm. And, the capture efficiency was found to level off at the channel length of 2 cm, which was chosen for subsequent experiments.

To investigate the general applicability of the 3D printed microfluidic devices, different human cancer cell lines (MCF-7 breast cancer, SW480 colon cancer, PC3 prostate cancer, and 293T kidney cancer) were tested and their capture efficiencies are shown in Fig. 5c. All MCF-7, SW480, and PC3 are EpCAM positive with resulting capture efficiencies of 92.42 ± 2.00%, 87.74 ± 1.22%, and 89.35 ± 1.21%, respectively. The slight differences between capture efficiencies were caused by varying degrees of EpCAM expression on the surfaces of each tumor cell line(Ahmed et al., 2017; Stott et al., 2010). As a negative control, capture efficiency as low as 26.14 ± 5.30% is observed for EpCAM negative cell line (293T). Conclusively, the anti-EpCAM antibody modified surfaces in the 3D printed microfluidic devices can specifically capture EpCAM-positive tumor cells at the capture efficiencies of around 90%.

3.6. Capturing CTCs from spiked whole blood samples

Artificial patient blood samples were made to validate the capture efficacy of our 3D printed microfluidic devices. The EDTA anticoagulated whole blood was collected from a healthy donor in the University Health Center at the University of California, Berkeley and used without any pre-treatment within 48 h. Instead of MCF-7 cells, MCF-7/GFP cells (with green fluorescent protein) were spiked into the whole blood. While pre-processing blood samples (density-gradient centrifugation) can minimize the sample volume and shorten experiment time, CTCs could potentially be lost during the process to result in lower capture efficiencies(Qasaimeh et al., 2017). In this study, MCF-7/GFP tumor cells were spiked into whole blood, which were directly injected into the anti-EpCAM antibody functionalized 3D printed microfluidic devices without any sample preparation. The artificially spiked blood samples before and after flowing through the 3D printed microfluidic devices were characterized using CLSM (in Fig. 6a–b), where fluorescence images were used to quantify MCF-7/GFP (green color) and brightfield images were used to quantify blood cells. As the negative and positive controls, MCF-7/GFP in PBS and blood sample were also imaged (Figs. S2a–b). The number of blood cells and MCF-7/GFP tumor cells were counted from 5 randomly picked images and plotted in Fig. 6c and d, respectively. It is found that the number of blood cells remained consistent before and after the isolation process, indicating that our devices have negligible specific bindings to blood cells. On the other hand, the tumor cell number significantly decreased in the output blood solutions (Fig. 6d). After the capture process, tumor cell numbers were found to be less than five counts per image, implying an average capture efficiency of MCF-7/GFP as high as 95% in the blood samples. We have tested three devices and the results were consistent over these devices. These results demonstrate that our anti-EpCAM antibody functionalized 3D printed microfluidic

devices exhibit great performance toward the specific capture of MCF-7 tumor cells in whole blood samples for potential promises toward clinical applications.

The major challenge in this field is the low concentration of CTCs in the blood. Since our prototype 3D device is not transparent, it is not possible to image and examine the captured cells directly, especially for cells with low concentrations. Alternatively, we estimate the capture efficiency by counting the cell concentration difference before and after the isolation process by a high cell concentration of 10^6 cells/mL. We believe the cell capture efficiency results could be extended for those at low concentrations. Although similar capture efficacities have been reported in the previous publications using conventional fabrication processes, they are generally limited for applications in laboratory settings with simple 2D-based structures. (Table S1). (Ahmed et al., 2017; Cheng et al., 2015; Earhart et al., 2014; Kim et al., 2013; Myung and Hong, 2015) Manufacturability with high-throughput and low-cost is important for practical applications, while true 3D geometry opens up the possibility of a variety of complex structures with high surface areas and features for better CTC capture efficiencies. 3D printed prototypes as presented in this work demonstrate the feasibility toward these directions.

4. Conclusion

In conclusion, we have demonstrated a 3D printed CTC-capture microfluidic device to dramatically increase the surface area with manipulated fluid flow patterns to improve the contact interactions between the tumor cell and 3D printed inner structures. The inner structures are then functionalized with anti-EpCAM antibodies to provide specific capture of EpCAM positive human cancer cell lines (such as, MCF-7 breast cancer, SW480 colon cancer, and PC3 prostate cancer). The results show CTC-capture efficiencies up to 92.42 ± 2.00% for MCF-7, 87.74 ± 1.22% for SW480, and 89.35 ± 1.21% for PC3 cells Furthermore, the 3D printed microfluidic devices have been demonstrated to isolate CTCs from artificial blood samples. In combination with enzymatic lysis of the captured tumor cells and the analysis of the released DNA in the blood, the 3D printed microfluidic technique could open up opportunities for the isolation of rare tumor cells and early detection of cancer metastasis.

Supplementary Material

Refer to Web version on PubMed Central for supplementary material.

Acknowledgement

We thank the Hangzhou Wahaha Group Co., Ltd. (China) for supporting this research financially. Additional thanks go to Professor Lydia Sohn in the Dept. of Mechanical Engineering at the University of California, Berkeley for providing human breast cancer cell line (MCF-7/GFP).

References

Ahmed MG, Abate MF, Song Y, Zhu Z, Yan F, Xu Y, Wang X, Li Q, Yang CJ, 2017. Isolation, detection and antigen based profiling of circulating tumor cells using a size dictated immunocapture chip. Angew. Chem. Int. Ed. 56, 10681–10685.

Au AK, Huynh W, Horowitz LF, Folch A, 2016. 3D-Printed microfluidics. Angew. Chem. Int. Ed. 55 (12), 3862–3881.

Au AK, Lee W, Folch A, 2014. Mail-order microfluidics: evaluation of stereolithography for the production of microfluidic devices. Lab Chip 14 (7), 1294–1301. [PubMed: 24510161]

Bhattacharjee N, Urrios A, Kanga S, Folch A, 2016. The upcoming 3D-printing revolution in microfluidics. Lab Chip 16 (10), 1720–1742. [PubMed: 27101171]

Chan HN, Tan MJA, Wu HK, 2017. Point-of-care testing: applications of 3D printing. Lab Chip 17 (16), 2713–2739. [PubMed: 28702608]

Chen J, Li Y, Huang K, Wang P, He L, Carter KR, Nugen SR, 2015. Nanoimprinted patterned pillar substrates for surface-enhanced Raman scattering applications. ACS Appl. Mater. Interfaces 7 (39), 22106–22113. [PubMed: 26402032]

Chen J, Zhou Y, Wang D, He F, Rotello VM, Carter KR, Watkins JJ, Nugen SR, 2015. UV-nanoimprint lithography as a tool to develop flexible microfluidic devices for electrochemical detection. Lab Chip 15 (14), 3086–3094. [PubMed: 26095586]

Chen YC, Li P, Huang PH, Xie YL, Mai JD, Wang L, Nguyen NT, Huang TJ, 2014. Rare cell isolation and analysis in microfluidics. Lab Chip 14 (4), 626–645. [PubMed: 24406985]

Cheng IF, Huang WL, Chen TY, Liu CW, Lin YD, Su WC, 2015. Antibody-free isolation of rare cancer cells from blood based on 3D lateral dielectrophoresis. Lab Chip 15 (14), 2950–2959. [PubMed: 26085231]

Earhart CM, Hughes CE, Gaster RS, Ooi CC, Wilson RJ, Zhou LY, Humke EW, Xu LY, Wong DJ, Willingham SB, Schwartz EJ, Weissman IL, Jeffrey SS, Neal JW, Rohatgi R, Wakeleebe HA, Wang SX, 2014. Isolation and mutational analysis of circulating tumor cells from lung cancer patients with magnetic sifters and biochips. Lab Chip 14 (1), 78–88. [PubMed: 23969419]

Gleghorn JP, Pratt ED, Denning D, Liu H, Bander NH, Tagawa ST, Nanus DM, Giannakakou PA, Kirby BJ, 2010. Capture of circulating tumor cells from whole blood of prostate cancer patients using geometrically enhanced differential immunocapture (GEDI) and a prostate-specific antibody. Lab Chip 10 (1), 27–29. [PubMed: 20024046]

Jackson JM, Witek MA, Kamande JW, Soper SA, 2017. Materials and microfluidics: enabling the efficient isolation and analysis of circulating tumour cells. Chem. Soc. Rev. 46 (14), 4245–4280. [PubMed: 28632258]

Kim S, Han SI, Park MJ, Jeon CW, Joo YD, Choi IH, Han KH, 2013. Circulating tumor cell microseparator based on lateral magnetophoresis and immunomagnetic nanobeads. Anal. Chem. 85 (5), 2779–2786. [PubMed: 23384087]

Ku SH, Lee JS, Park CB, 2010. Spatial control of cell adhesion and patterning through mussel-inspired surface modification by polydopamine. Langmuir 26 (19), 15104–15108. [PubMed: 20806924]

Kurkuri MD, Al-Ejeh F, Shi JY, Palms D, Prestidge C, Griesser HJ, Brown MP, Thierry B, 2011. Plasma functionalized PDMS microfluidic chips: towards point-of-care capture of circulating tumor cells. J. Mater. Chem. 21 (24), 8841–8848.

Lee H, Dellatore SM, Miller WM, Messersmith PB, 2007. Mussel-inspired surface chemistry for multifunctional coatings. Science 318 (5849), 426–430. [PubMed: 17947576]

Lee H, Rho J, Messersmith PB, 2009. Facile conjugation of biomolecules onto surfaces via mussel adhesive protein inspired coatings. Adv. Mater. 21 (4), 431–434. [PubMed: 19802352]

Lin E, Rivera-Baez L, Fouladdel S, Yoon HJ, Guthrie S, Wieger J, Deol Y, Keller E, Sahai V, Simeone DM, Burness ML, Azizi E, Wicha MS, Nagrath S, 2017. High-throughput microfluidic labyrinth for the label-free isolation of circulating tumor cells. Cell. Syst. 5 (3), 295–304. [PubMed: 28941584]

Li YQ, Chandran BK, Lim CT, Chen XD, 2015. Rational design of materials interface for efficient capture of circulating tumor cells. Adv. Sci. 2 (11), 1500118.

Li YY, Lu QH, Liu HL, Wang JF, Zhang PC, Liang HG, Jiang L, Wang ST, 2015. Antibody-modified reduced graphene oxide films with extreme sensitivity to circulating tumor cells. Adv. Mater. 27 (43), 6848–6854. [PubMed: 26426823]

Lin M, Chen JF, Lu YT, Zhang Y, Song J, Hou S, Ke Z, Tseng HR, 2014. Nanostructure embedded microchips for detection, isolation, and characterization of circulating tumor cells. Acc. Chem. Res. 47 (10), 2941–2950. [PubMed: 25111636]

Lynge ME, van der Westen R, Postma A, Städler B, 2011. Polydopamine—a nature-inspired polymer coating for biomedical science. Nanoscale 3 (12), 4916–4928. [PubMed: 22024699]

Miller MC, Doyle GV, Terstappen LW, 2010. Significance of circulating tumor cells detected by the CellSearch system in patients with metastatic breast colorectal and prostate cancer. J. Oncol. 2010, 617421. [PubMed: 20016752]

Murlidhar V, Rivera-Baez L, Nagrath S, 2016. Affinity versus label-free isolation of circulating tumor cells: who wins? Small 12 (33), 4450–4463. [PubMed: 27436104]

Murlidhar V, Zeinali M, Grabauskiene S, Ghannad-Rezaie M, Wicha MS, Simeone DM, Ramnath N, Reddy RM, Nagrath S, 2014. A radial flow microfluidic device for ultra-high-throughput affinity-based isolation of circulating tumor cells. Small 10 (23), 4895–4904. [PubMed: 25074448]

Myung JH, Hong S, 2015. Microfluidic devices to enrich and isolate circulating tumor cells. Lab Chip 15 (24), 4500–4511. [PubMed: 26549749]

Nagrath S, Sequist LV, Maheswaran S, Bell DW, Irimia D, Ulkus L, Smith MR, Kwak EL, Digumarthy S, Muzikansky A, Ryan P, Balis UJ, Tompkins RG, Haber DA, Toner M, 2007. Isolation of rare circulating tumour cells in cancer patients by microchip technology. Nature 450 (7173), 1235–1239. [PubMed: 18097410]

Pantel K, Alix-Panabières C, 2013. Real-time liquid biopsy in cancer patients: fact or fiction? Cancer Res. 73 (21), 6384–6388. [PubMed: 24145355]

Park ES, Jin C, Guo Q, Ang RR, Duffy SP, Matthews K, Azad A, Abdi H, Todenhofer T, Bazov J, Chi KN, Black PC, Ma HS, 2016. Continuous flow deformability-based separation of circulating tumor cells using microfluidic ratchets. Small 12 (14), 1909–1919. [PubMed: 26917414]

Qasaimeh MA, Wu YCC, Bose S, Menachery A, Talluri S, Gonzalez G, Fulciniti M, Karp JM, Prabhala RH, Karnik R, 2017. Isolation of circulating plasma cells in multiple myeloma using CD138 antibody-based capture in a microfluidic device. Sci. Rep. 7, 45681. [PubMed: 28374831]

Reategui E, Aceto N, Lim EJ, Sullivan JP, Jensen AE, Zeinali M, Martel JM, Aranyosi AJ, Li W, Castleberry S, Bardia A, Sequist LV, Haber DA, Maheswaran S, Hammond PT, Toner M, Stott SL, 2015. Tunable nanostructured coating for the capture and selective release of viable circulating tumor cells. Adv. Mater. 27 (9), 1593. [PubMed: 25640006]

Riethdorf S, Müller V, Zhang L, Rau T, Loibl S, Komor M, Roller M, Huober J, Fehm T, Schrader I, 2010. Detection and HER2 expression of circulating tumor cells: prospective monitoring in breast cancer patients treated in the neoadjuvant GeparQuattro trial. Clin. Cancer Res. 16 (9), 2634–2645. [PubMed: 20406831]

Sackmann EK, Fulton AL, Beebe DJ, 2014. The present and future role of microfluidics in biomedical research. Nature 507, 181–189. [PubMed: 24622198]

Sarioglu AF, Aceto N, Kojic N, Donaldson MC, Zeinali M, Hamza B, Engstrom A, Zhu H, Sundaresan TK, Miyamoto DT, Luo X, Bardia A, Wittner BS, Ramaswamy S, Shioda T, Ting DT, Stott SL, Kapur R, Maheswaran S, Haber DA, Toner M, 2015. A microfluidic device for label-free, physical capture of circulating tumor cell clusters. Nat. Methods 12 (7), 685–+. [PubMed: 25984697]

Shah P, Zhu X, Chen C, Hu Y, Li C-Z, 2014. Lab-on-chip device for single cell trapping and analysis. Biomed. Microdevices 16 (1), 35–41. [PubMed: 23948962]

Sochol RD, Sweet E, Glick CC, Venkatesh S, Avetisyan A, Ekman KF, Raulinaitis A, Tsai A, Wienkers A, Korner K, Hanson K, Long A, Hightower BJ, Slatton G, Burnett DC, Massey TL, Iwai K, Lee LP, Pister KSJ, Lin L, 2016. 3D printed microfluidic circuitry via multijet-based additive manufacturing. Lab Chip 16 (4), 668–678. [PubMed: 26725379]

Stott SL, Hsu CH, Tsukrov DI, Yu M, Miyamoto DT, Waltman BA, Rothenberg SM, Shah AM, Smas ME, Korir GK, Floyd FP Jr., Gilman AJ, Lord JB, Winokur D, Springer S, Irimia D, Nagrath S, Sequist LV, Lee RJ, Isselbacher KJ, Maheswaran S, Haber DA, Toner M, 2010. Isolation of circulating tumor cells using a microvortex-generating herringbone-chip. Proc. Natl. Acad. Sci. U. S. A. 107 (43), 18392–18397. [PubMed: 20930119]

Sun JS, Li MM, Liu C, Zhang Y, Liu DB, Liu WW, Hu GQ, Jiang XY, 2012. Double spiral microchannel for label-free tumor cell separation and enrichment. Lab Chip 12 (20), 3952–3960. [PubMed: 22868446]

Talasaz AH, Powell AA, Huber DE, Berbee JG, Roh K-H, Yu W, Xiao W, Davis MM, Pease RF, Mindrinos MN, 2009. Isolating highly enriched populations of circulating epithelial cells and

other rare cells from blood using a magnetic sweeper device. Proc. Natl. Acad. Sci. 106 (10), 3970–3975. [PubMed: 19234122]

Tseng P, Murray C, Kim D, Di Carlo D, 2014. Research highlights: printing the future of microfabrication. Lab Chip 14 (9), 1491–1495. [PubMed: 24671475]

Wang S, Liu K, Liu J, Yu ZTF, Xu X, Zhao L, Lee T, Lee EK, Reiss J, Lee Y-K, Chung LWK, Huang J, Rettig M, Seligson D, Duraiswamy KN, Shen CKF, Tseng H-R, 2011. Highly efficient capture of circulating tumor cells by using nanostructured silicon substrates with integrated chaotic micromixers. Angew. Chem. Int. Ed. 50 (13), 3084–3088.

Wu J, Chen Q, Lin JM, 2017. Microfluidic technologies in cell isolation and analysis for biomedical applications. Analyst 142 (3), 421–441. [PubMed: 27900377]

Wu L, Wang J, Ren J, Qu X, 2014. Ultrasensitive telomerase activity detection in circulating tumor cells based on DNA metallization and sharp solid-state electrochemical techniques. Adv. Funct. Mater. 24 (18), 2727–2733.

Yoon HJ, Shanker A, Wang Y, Kozminsky M, Jin Q, Palanisamy N, Burness ML, Azizi E, Simeone DM, Wicha MS, Kim JS, Nagrath S, 2016. Tunable thermal-sensitive polymer-graphene oxide composite for efficient capture and release of viable circulating tumor cells. Adv. Mater. 28 (24), 4891–4897. [PubMed: 27115557]

Zhang P, He M, Zeng Y, 2016. Ultrasensitive microfluidic analysis of circulating exosomes using a nanostructured graphene oxide/polydopamine coating. Lab Chip 16 (16), 3033–3042. [PubMed: 27045543]

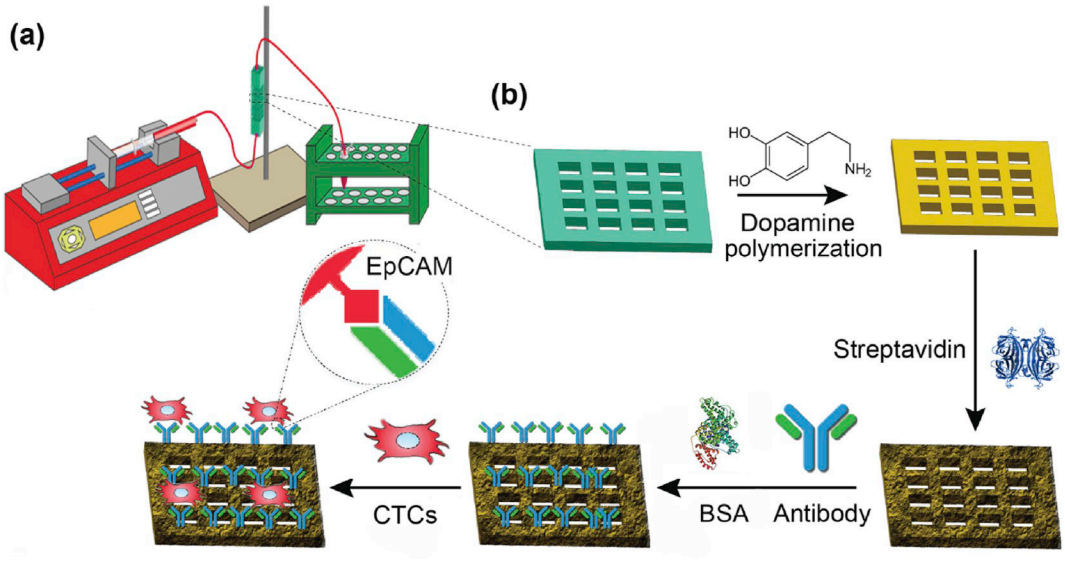

Fig. 1.

(a) Schematic illustration of the setup pf microfluidic platform, and (b) schematic representation of surface modification chemistry and anti-EpCAM antibody immobilization procedures.

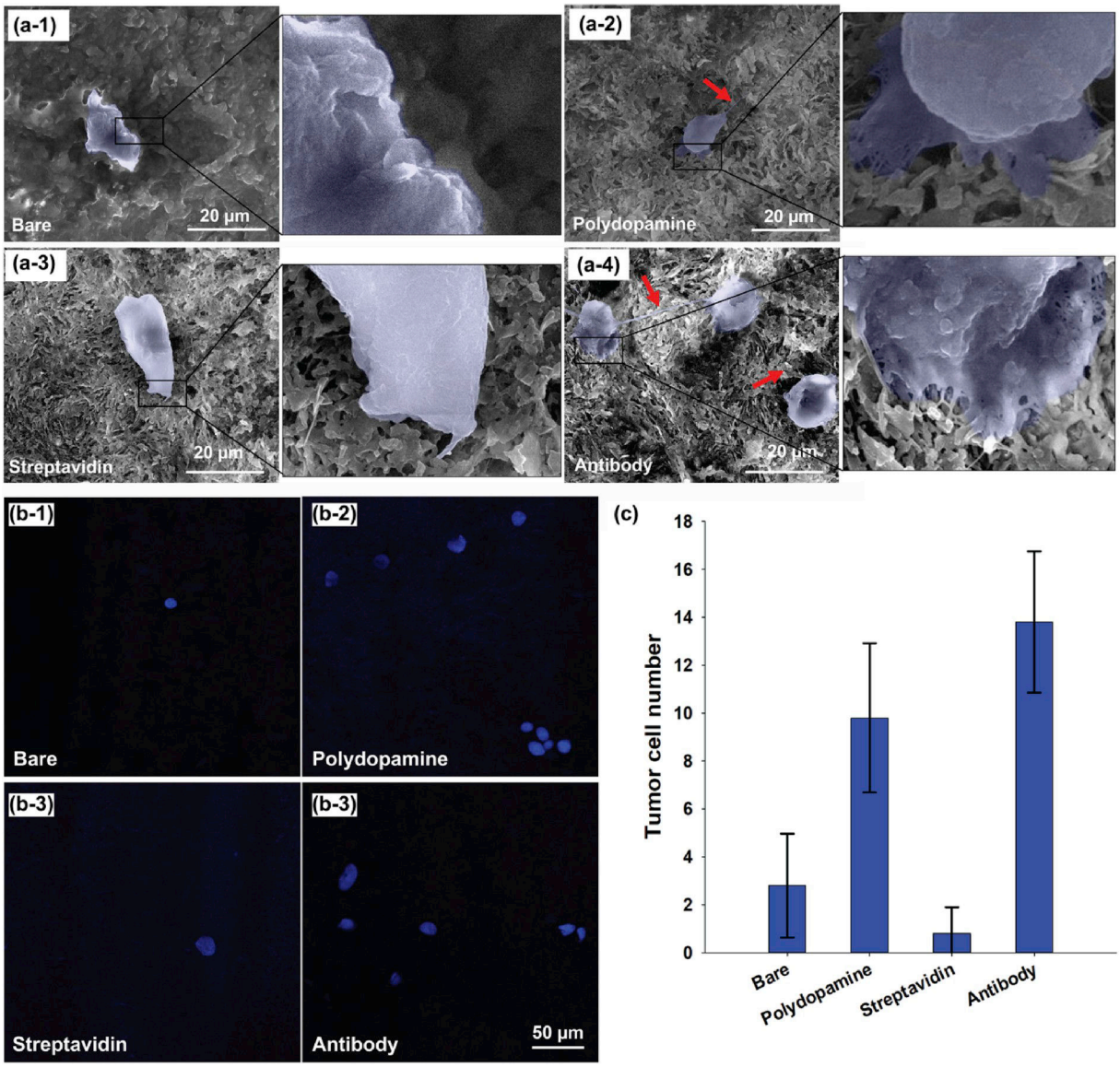

Fig. 2.

(a) SEM images of the captured tumor cells (breast cancer cell line, MCF-7) on 3D printed material surface after different modifications, and (b) confocal fluorescent images and (c) quantification of the captured tumor cells (breast cancer cell line, MCF-7) after different surface modifications.

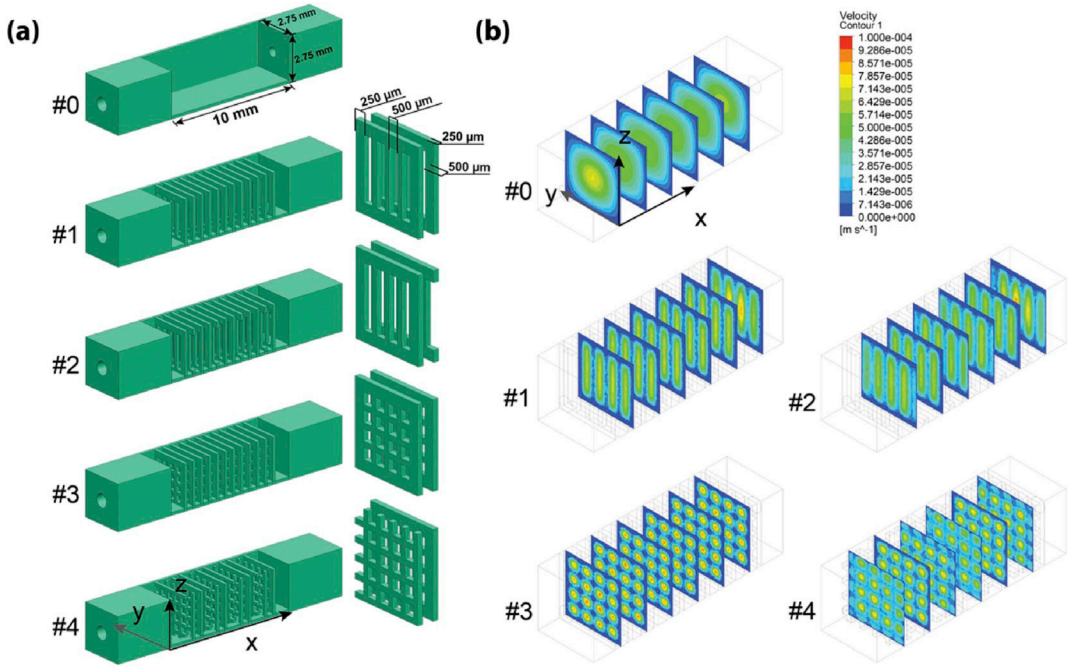

Fig. 3.

(a) Designs of five different 3D printed microfluidic devices (inserted images are the inner structures) and (b) velocity magnitude profiles of five different designs.

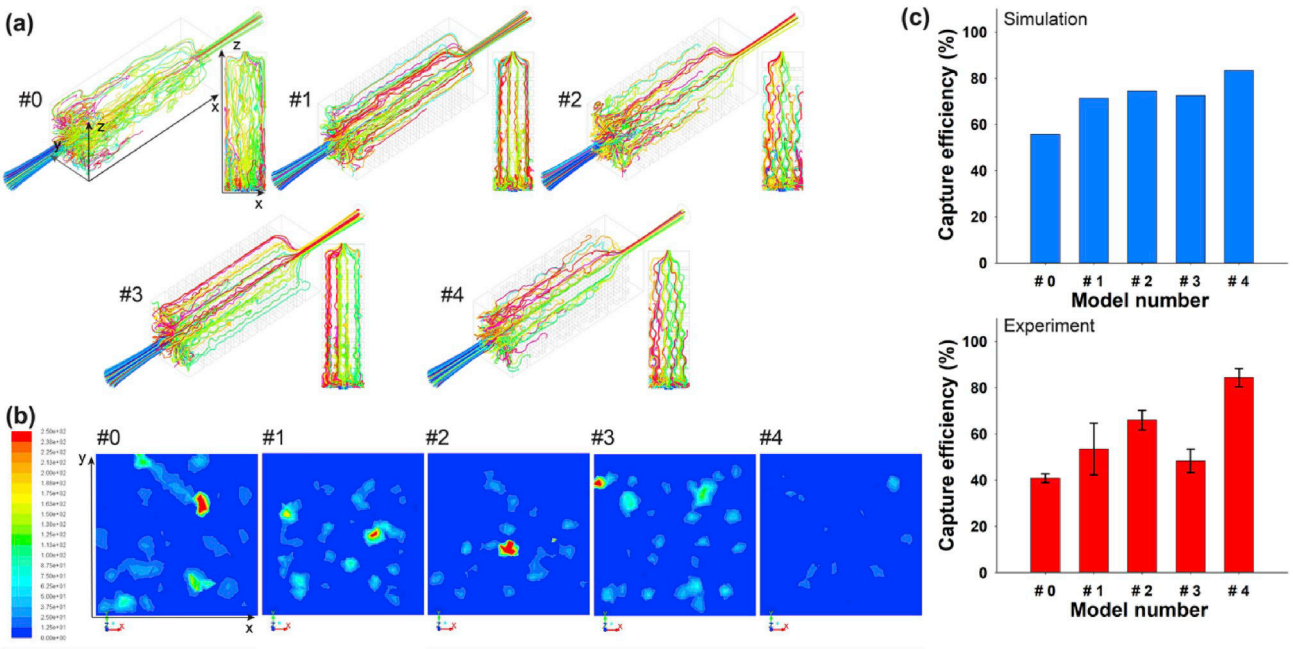

Fig. 4.

(a) Simulated particle tracing within five different 3D printed microfluidic devices (inserted images are the cross-section of simulated particle tracing), (b) the Z-axis side view of the simulated particle tracing in the last layer, and (c) capture efficiency between simulation and experimental results on tumor cell isolation.

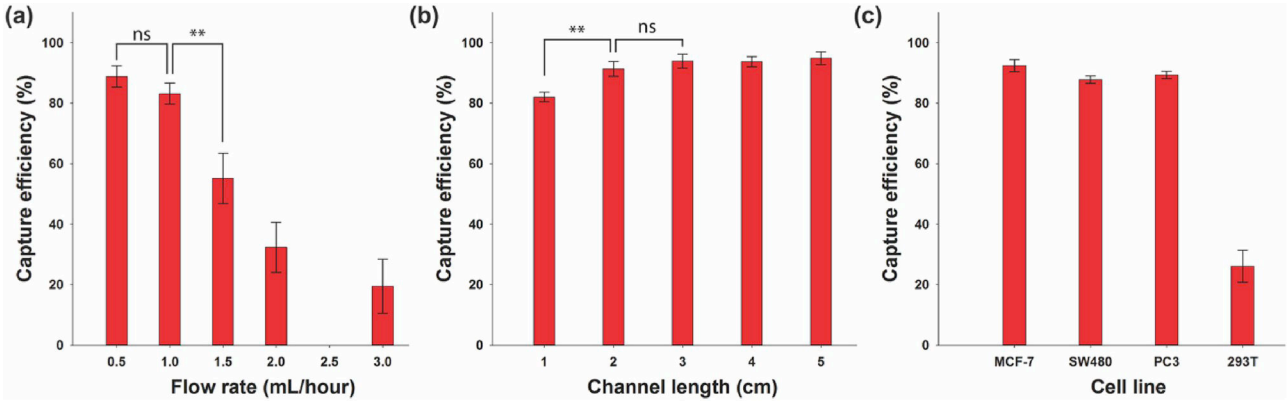

Fig. 5.

Capture efficiency optimization (a) at flow rate of 0.5, 1.0, 1.5, 2.0, and 3.0 mL/h and (b) using channel length from 1 to 5 cm, (c) the selectivity of anti-EpCAM functionalized 3D printed microfluidic device on breast cancer (MCF-7), colon cancer (SW480), prostate cancer (PC3), and kidney cancer (293T).

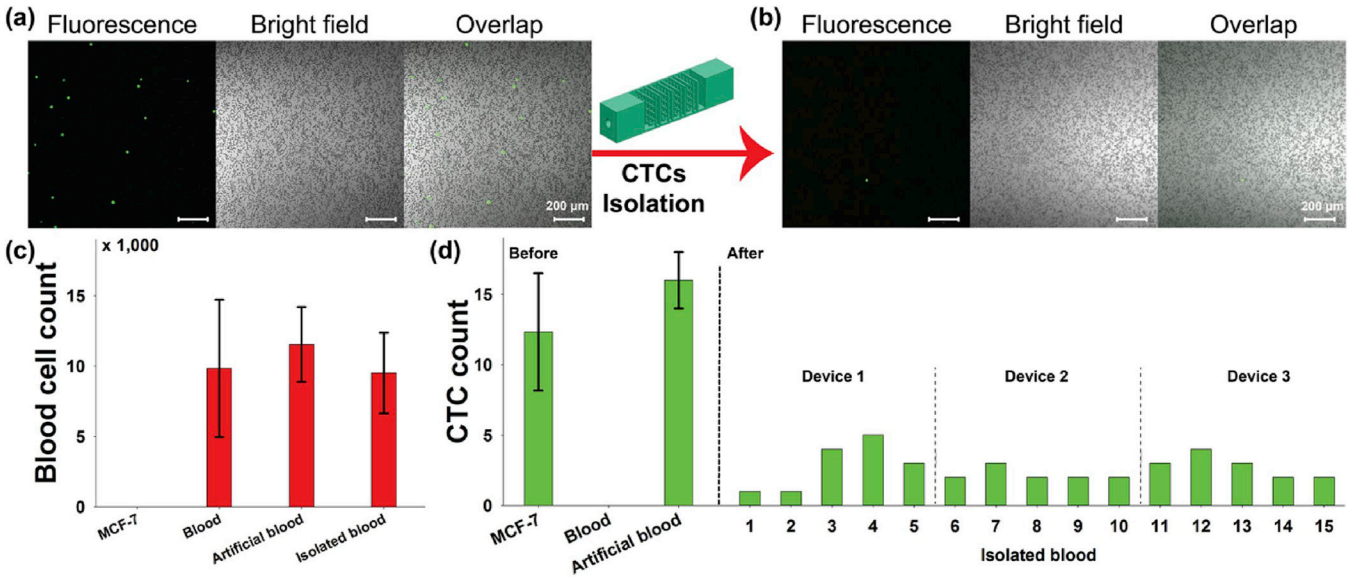

Fig. 6.

Fluorescence microscopy image and quantification of CTCs isolation from blood samples. (a–b) Fluorescence and brightfield images of artificial patient blood samples before and after isolation, respectively. (c) quantification of blood cells from artificial patient blood sample, and (d) quantification of CTCs from artificial patient blood samples.